

Curriculum Learning for LLM Pretraining

An Analysis of Learning Dynamics

Mohamed Elgaar¹ Hadi Amiri¹

Abstract

Curriculum learning changes the order of pre-training data, but it remains unclear whether it changes the learning trajectory or mainly reorders exposure over a fixed trajectory. We train Pythia models (14M–410M parameters) for 300B tokens under three linguistically motivated curricula—Age-of-Acquisition, word frequency, and Verb Variation (VV)—and compare each against Random ordering; at 1B parameters we compare Random and VV. Across orderings, training follows a shared sequence of latent phases, while curricula mainly change within-phase data exposure. In smaller models (up to 160M parameters), Random ordering exhibits higher gradient noise and stronger late-training output-head spectral saturation, alongside lower final accuracy; curricula reduce both effects at matched compute. At larger scales, saturation differences are smaller and curriculum gains shrink. We formalize the link between difficulty pacing and optimization stability in an idealized analysis based on gradient-variance control, and our results point to a practical takeaway: curricula help by stabilizing within-phase optimization rather than by creating new phases.¹

1. Introduction

Pretraining large language models requires substantial compute, often on the order of hundreds of petaflop-days per run (Kaplan et al., 2020; Hoffmann et al., 2022). Accordingly, modern practice typically trains for a single epoch over massive corpora: revisiting data is inefficient when new data are abundant (Komatsuzaki, 2019). Compute-optimal scaling laws similarly treat the budget as the total number of tokens consumed from a unique corpus (Hoffmann et al.,

¹University of Massachusetts Lowell, MA, USA. Correspondence to: Mohamed Elgaar <mohamed_elgaar@uml.edu>.

2022). In this single-pass setting, data ordering is consequential: each sample is encountered exactly once. Curriculum learning—presenting training examples in a structured order, often easy-to-hard—offers a way to shape this process (Bengio et al., 2009; Elman, 1993). One motivation is that learning may be easier when foundational patterns come before rarer or more complex ones.

Despite this intuition, results on curriculum learning for LLM pretraining are mixed. Some studies report gains at fixed compute budgets (Fan & Jaggi, 2023), whereas others find diminishing or negligible effects at scale (Campos, 2021). One reason is that it remains unclear which aspects of training dynamics curricula affect. Curricula could either change the learning trajectory—the sequence of internal states a model traverses during training—or primarily change which data the model sees at each stage without altering the underlying dynamics. To design curricula that improve training consistently, we need to separate these possibilities.

This distinction matters most for smaller models, where capacity constraints make the interaction between data ordering and learning dynamics particularly consequential. These models face structural limits such as the softmax bottleneck (Godey et al., 2024; Michaelov & Bergen, 2023)—where a low-rank output head cannot represent the high-rank distributions required for language modeling. As training progresses, this mismatch can cause late-stage degradation, and its interaction with data ordering may not be apparent from end-point aggregates such as final loss or benchmark accuracy.

We address these questions with a systematic study of data ordering in LLM pretraining. We train Pythia models (14M–410M parameters) for 300B tokens under three linguistically motivated curricula—Age-of-Acquisition, word frequency, and Verb Variation (VV)—and compare them against Random ordering; for 1B parameters, we compare Random and VV due to compute constraints. Beyond aggregate metrics, we analyze learning dynamics in two ways. First, we perform latent phase analysis by fitting Hidden Markov Models to training trajectories. Second, we track optimization diagnostics: the gradient noise scale (McCandlish et al., 2018), a measure of gradient signal-to-noise ratio, and singular

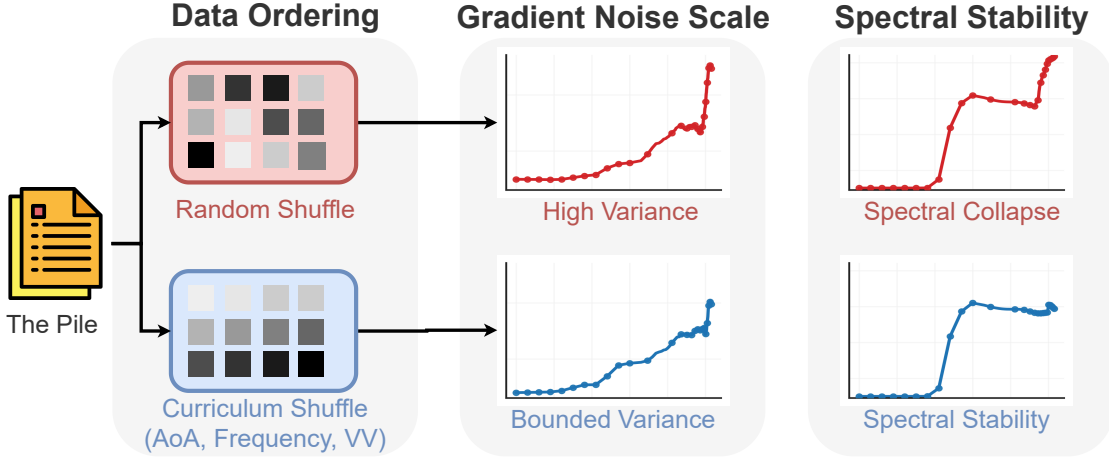


Figure 1. Overview of the mechanism studied in this work. In smaller, capacity-constrained models, random data ordering can produce higher gradient noise scale, coinciding with late-stage spectral saturation of the output head. Linguistically motivated curricula (Age-of-Acquisition, Frequency, and Verb Variation) reduce gradient noise and are associated with improved spectral stability.

entropy (Godey et al., 2024), which quantifies spectral saturation of the output head. We summarize the mechanism in Figure 1.

Across all orderings, training follows a shared sequence of latent phases. Curricula mainly change which data appears within each phase. The effect is strongest at small scales: for smaller models (14M–70M), Random ordering exhibits higher gradient noise scale; for models up to 160M, it also shows stronger late-training spectral saturation. Curricula reduce both effects and can improve accuracy at matched compute. At larger scales (410M+), these differences diminish and curriculum gains become marginal.

This paper makes the following contributions:

- We show that pretraining trajectories under different data orderings share a consistent latent phase structure. Using a joint HMM analysis across orderings (illustrated for the 14M model, and with multiple random seeds for small models), we find that curricula mainly reshape within-phase data exposure rather than changing the phase sequence.
- We provide a theoretical framework formalizing curriculum learning as a stability mechanism (Theorem 3.2): by controlling the difficulty of data encountered over training, curricula can bound gradient variance and reduce late-stage optimization instability.
- We demonstrate empirically that curricula reduce gradient noise scale and output-head spectral saturation in smaller models. These reductions align with weaker late-stage effects that we associate with the softmax bottleneck, and they diminish at larger scales where capacity is sufficient to avoid saturation.

- We report experiments spanning five model sizes (14M–410M) trained for 300B tokens under three linguistically grounded curricula and Random ordering, with additional 1B runs for Random and VV, showing that curriculum gains are scale-dependent and most pronounced for capacity-constrained models.

2. Related Work

We build on three research threads: curriculum learning for language model pretraining, analyses of training dynamics, and scaling effects. Curriculum learning orders examples to shape optimization, classically in easy-to-hard form (Bengio et al., 2009; Elman, 1993). While many curriculum formulations and schedules have been proposed (Cornacchia & Mossel, 2023; Kong et al., 2021; Zhou & Bilmes, 2018), their implications are less clear in single-pass LLM pretraining. Empirical findings are mixed: linguistically motivated orderings can show diminishing returns at scale (Campos, 2021), whereas proxy-learnability orderings can improve perplexity and downstream accuracy for larger models (Fan & Jaggi, 2023); length-based curricula may affect stability with uncertain effects on final quality (Li et al., 2022; Nagatsuka et al., 2023).

To capture within-training changes that aggregate metrics obscure (Kaplan et al., 2020; Hoffmann et al., 2022), we model training trajectories with Hidden Markov Models. Prior approaches analyze trajectories via data attribution (Koh & Liang, 2017; Pruthi et al., 2020) or simulate sequence effects on metric evolution under different data orderings (Guu et al., 2023; Chai et al., 2024). HMMs have been used to identify consistent learning phases across random seeds (van der Wal et al., 2025); we extend this by fitting a joint HMM across orderings to test whether curric-

ula change phase structure or primarily reallocate exposure within shared phases.

To connect ordering to mechanisms, we focus on stability diagnostics and late-stage capacity limits. Gradient noise scale provides an optimization-stability lens (McCandlish et al., 2018), and the softmax bottleneck highlights how small models can saturate or degrade late in training due to limited-rank output heads (Godey et al., 2024; Michaelov & Bergen, 2023). We connect these threads by showing that curricula largely preserve the phase sequence but shift within-phase exposure, and that these shifts coincide with improved late-phase stability as measured by gradient noise and spectral summaries of the language-modeling head.

3. Theoretical Framework for Curriculum Learning

We study curriculum learning as a mechanism for preventing late-stage performance degradation, rather than for accelerating early learning. We model a curriculum as a parameterized sampling mechanism (via difficulty scores and pacing functions) and analyze its effect on optimization stability through the variance of stochastic gradients. Throughout this section, the training objective is modeled as a population risk

$$F(\theta) = \mathbb{E}_{z \sim \mathcal{P}}[\ell(\theta, z)],$$

where $\theta \in \mathbb{R}^{d_\theta}$ are the model parameters, z is a training example drawn from a data distribution \mathcal{P} , and ℓ is the per-example loss. Stochastic gradient descent (SGD) with a possibly time-varying sampling distribution \mathcal{P}_t performs updates

$$\theta_{t+1} = \theta_t - \eta g_t, \quad g_t = \nabla_\theta \ell(\theta_t, z_t), \quad z_t \sim \mathcal{P}_t, \quad (1)$$

with constant step size $\eta > 0$. We use standard convex-optimization assumptions (strong convexity and smoothness of F , unbiased gradients with bounded variance) to derive stability bounds. Although these assumptions are not exact for deep networks, they clarify the mechanisms we measure in §5.

3.1. The Softmax Bottleneck and Rank Saturation (details in appendix)

Small models can exhibit late-stage saturation effects due to the softmax bottleneck (Godey et al., 2024). We track output-head spectral degeneration using singular entropy and relate it to the stability mechanism in §5 (Figure 2). The formal lemma and the singular-entropy definition appear in Appendix A.

3.2. The Link Between Ideal Difficulty and Gradient Variance

Hacohen & Weinshall (2019) advocate training first on examples with low loss under the optimal model θ^* . We link this static notion of difficulty to gradient-variance differences during SGD.

Definition 3.1 (Ideal Difficulty Score). Following Weinshall et al. (2018), the *ideal difficulty score* of a training point z_i is its loss with respect to the optimal hypothesis θ^* , i.e., $\Psi_i = \ell(\theta^*, z_i)$.

We split the data into “easy” and “hard” subsets by thresholding Ψ_i and assume that, near θ^* , stochastic gradients on the hard subset have larger variance than those on the easy subset. Appendix A states this variance ordering formally; we use it to connect difficulty pacing to optimization stability.

3.3. The Gradient Noise Scale

The gradient noise scale (GNS) is a measure of the signal-to-noise ratio in stochastic gradient estimates (McCandlish et al., 2018). Let $G = \mathbb{E}[g_t \mid \theta_t] = \nabla F(\theta_t)$ denote the true gradient and $\Sigma = \text{cov}(g_t \mid \theta_t)$ the covariance of the stochastic gradient. The simplified noise scale is defined as

$$\mathcal{B} = \frac{\text{tr}(\Sigma)}{\|G\|_2^2}, \quad (2)$$

which measures the total gradient variance relative to the squared gradient magnitude. When \mathcal{B} is large, stochastic gradient estimates are dominated by noise, leading to inefficient optimization; when \mathcal{B} is small, gradients are more consistent across batches and optimization proceeds efficiently.

For a sampling distribution \mathcal{P}_t with effective gradient variance σ_t^2 , the noise scale satisfies $\mathcal{B}_t \propto \sigma_t^2 / \|G_t\|_2^2$. A curriculum that controls the evolution of σ_t^2 thus changes the noise scale, affecting optimization efficiency and late-phase stability. We expect curriculum-based orderings to yield lower GNS than Random ordering, especially late in training when uniform sampling exposes the optimizer to higher-difficulty examples. We test this in §5 and report full GNS trajectories in Figure 3.

3.4. Uniform Sampling and Difficulty Pacing (details in appendix)

The argument uses two assumptions: (i) under uniform sampling, training can drift toward higher-variance (harder) gradient contributions later in optimization; and (ii) curricula can be modeled as difficulty-based pacing rules that restrict which examples are exposed at each stage. Appendix A gives the mixture decomposition, the corresponding assumption about the late-stage increase of effective gradient variance, and a pacing-function definition.

3.5. Curriculum Learning as a Stability Mechanism

We next state a result showing that a curriculum (difficulty score plus pacing function) can improve SGD stability by controlling stochastic-gradient variance.

Standard SGD analysis shows that under strong convexity and Lipschitz gradients, the asymptotic stability radius scales with the gradient variance σ^2 : sampling schemes with bounded variance yield tighter stability bounds (Bottou et al., 2018; Garrigos & Gower, 2023). This motivates controlling variance via difficulty pacing. The formal lemma (Theorem A.6) and proof appear in Appendix A.

We now connect this bound to curricula defined by a difficulty score d and pacing function p .

Theorem 3.2 (Curriculum Learning and Stability (informal)). *In an idealized strongly convex setting, the stability radius of SGD scales with the effective gradient variance: sampling schemes that keep σ_t^2 bounded yield tighter stability bounds. Under uniform sampling, σ_t^2 may drift toward a high-variance regime late in training; curricula induced by difficulty pacing delay this drift by limiting exposure to high-variance examples early and increasing difficulty gradually. The full statement and proof are given in Appendix A.*

3.6. Mapping the framework to our curricula (difficulty score and pacing)

The framework above is parameterized by a difficulty score $d(z)$ and a pacing function $p(t)$ that together induce a time-varying sampling distribution \mathcal{P}_t . In our experiments, each curriculum defines a deterministic ordering over the one-epoch pretraining stream by sorting fixed-length 2048-token samples (Section 4). We map the framework to our setting and test Theorem 3.2 in §5: curricula should reduce gradient noise scale and improve late-phase stability relative to uniform (random) sampling.

Difficulty score $d(z)$. For each sample z , we set $d(z)$ to the curriculum’s scalar score: Age-of-Acquisition (AoA), word frequency, or Verb Variation (VV) as defined in Appendix E. Because the ideal difficulty Ψ_i in Definition 3.1 is too expensive to compute at scale, we treat these linguistic scores as proxies and show that they correlate with sample loss (Appendix E.3).

Pacing function $p(t)$. Let $t \in [0, 1]$ denote normalized training progress over a single pass through the data. For a fully sorted curriculum, a natural idealization is a linear pacing in quantiles of d : at progress t , the effective support of \mathcal{P}_t is restricted to the prefix of samples whose difficulty satisfies $d(z) \leq p(t)$, where $p(t)$ is the empirical t -quantile of d over the dataset. This corresponds to sampling predominantly from easier examples early and gradually expanding coverage to include harder examples. Under Random order-

ing, this mapping reduces to the time-invariant distribution $\mathcal{P}_t \equiv \mathcal{P}$ (equivalently, $p(t) = d_{\max}$ for all t), which is the uniform-sampling regime analyzed in Assumptions A.2–A.3.

4. Pretraining Curriculum Design

The curriculum operates at the level of individual training samples. Following the Pythia data processing pipeline (Biderman et al., 2023), documents from The Pile (Gao et al., 2020) are partitioned into fixed-size, 2048-token samples (Appendix E.1). We study a controlled setting in which this set of 2048-token samples is held fixed and only the ordering of samples is changed; differences in training dynamics can therefore be attributed to ordering rather than changes in the underlying sample set.

Each curriculum assigns a scalar score to every sample and sorts samples accordingly. A central challenge is choosing a score that approximates ideal difficulty while remaining tractable at scale. In line with Theorem 3.1, we want the score to correlate with sample loss. We use three inexpensive linguistic indices: Age-of-Acquisition (AoA) (Kuperman et al., 2012), word frequency using SUBTLEX_{US} and the Zipf scale (Brysbaert & New, 2009; Van Heuven et al., 2014), and Verb Variation (VV) (Guiraud, 1960). Across model scales, these indices correlate positively with sample loss (VV: 0.76; frequency: 0.73; AoA: 0.62), supporting their use as proxies for difficulty. These indices capture complementary linguistic signals: AoA reflects acquisition norms, frequency reflects lexical distributional statistics, and VV reflects verb-type diversity. We sort samples in ascending score (easy-to-hard in our setting). Details of scoring functions appear in Appendix E, and correlation analyses in Appendix E.3.

4.1. Linguistic Characterization of Curriculum Indices

Qualitative inspection of curriculum quantiles reveals systematic content differences. Low-score regions (low frequency, low AoA, low VV) tend to contain code, structured data, and specialized vocabulary; mid-range samples include expository and technical prose; high-score tails can contain repetitive or degenerate content (e.g., keyword lists, verb lexicons). VV should be interpreted as detected verb-type diversity rather than a pure measure of semantic complexity, since verb-list formats can dominate the extreme tail. These patterns help explain probe-level differences in §5; see Appendix E.4 for representative excerpts.

4.2. Models and Training Setup

The experiments use the Pythia suite (Biderman et al., 2023), specifically models with 14M, 31M, 70M, 160M, 410M, and 1B parameters. We use Pythia because it provides a standard

ized architecture and logging across model sizes, enabling controlled comparisons of data orderings; we also compare against stability analyses such as PolyPythias (van der Wal et al., 2025). The training setup replicates the original Pythia configuration, including learning rate, batch size, and optimizer, and these hyperparameters are held fixed across orderings for comparability.

For model sizes 14M–410M, we train separate runs from scratch under four orderings: Random ordering (a single random shuffle of The Pile) and three easy-to-hard curricula induced by Age-of-Acquisition, word frequency, and VV. Models are trained for 20B, 60B, and 300B tokens. These durations allow observation of dynamics within and across key learning phases identified in prior stability research (e.g., an initial phase typically concluding around 20B tokens, and a development phase extending from 20B to around 200B tokens (van der Wal et al., 2025)). For 1B parameters, due to compute constraints, we train and evaluate only Random and VV.

Detailed computational costs are provided in Appendix D. Training the 70M, 160M, and 410M models consumed approximately 530, 1,140, and 2,730 A100 GPU-hours, respectively. The 300B-token runs are necessary to expose late-stage behavior, enable the HMM to observe complete phase sequences, and assess final performance in a realistic single-epoch regime; shorter runs would suppress the saturation effects central to our hypothesis.

4.3. Analyzing Learning Dynamics

The influence of curricula on learning is examined from two perspectives: the evolution of external linguistic capabilities and the internal state of the model.

HMM-based Identification of Learning Phases Capability visualizations indicate what the model learns but provide limited insight into training stability and internal state transitions. We model training trajectories with a Hidden Markov Model (HMM) following Hu et al. (2023) to obtain a low-dimensional, discrete training map that facilitates identification of common learning phases and analysis of how curricula affect traversal of these phases.

Direct HMM fitting on the high-dimensional weight space is computationally infeasible. Instead, a small set of metrics is computed from the model’s weights at each checkpoint (Appendix G), capturing properties of the weight distribution (e.g., L_1 and L_2 norms) and the function computed by each layer (e.g., singular values). Time series of these metrics from multiple runs across curricula (and, for selected model sizes, across random seeds) are standardized with z-score normalization and used as observation sequences.

Full-length pretraining runs are expensive, so unless other-

wise noted we report one training replicate (seed 1234) per model size and data ordering. To ensure the HMM-based phase analysis reflects stable learning dynamics rather than idiosyncrasies of a single run, we train three seeds for the 14M and 31M models. These extra replicates let us test whether curriculum orderings versus Random ordering exhibit distinct but internally consistent latent-state sequence patterns across seeds.

We fit a Gaussian HMM to these sequences using the standard expectation-maximization procedure (Baum-Welch). As in van der Wal et al. (2025), we use five latent states: across model sizes, this choice is near-optimal under the Bayesian Information Criterion. Fixing the number of states supports direct comparisons across orderings. We train a single HMM jointly across the Age-of-Acquisition, Frequency, Verb Variation, and Random orderings so that phases are directly comparable.

The trained HMM provides a state transition diagram that functions as a training map and reveals a sequence of latent learning phases shared across orderings. The subsequent analysis assesses whether curricula change which states are visited—largely they do not—or instead alter the data processed within shared states, with implications for stability and performance, particularly late in training for smaller models.

In all runs, the HMM is fitted to 14 checkpoint-level observation metrics capturing: weight dispersion (average L_1/L_2 norms over weight matrices, L_1/L_2 ratio, means/medians/variances of weights and biases), and layer function (average trace, spectral norm, trace-to-spectral-norm ratio, and the mean/variance of singular values). These metrics summarize both parameter distribution and induced layer behavior. The complete list appears in Appendix G.

Evaluation Benchmarks The analysis relies on visualizations that track multiple capability-specific metrics throughout training. To capture the development of diverse linguistic and reasoning abilities, each model checkpoint is evaluated on benchmarks covering question answering, long-range context comprehension, logical reasoning, and commonsense understanding. Descriptions appear in Appendix F.

5. Results

Ordering effects depend on model scale Table 1 shows that no single ordering dominates downstream benchmark accuracy across scales. Frequency attains the best average score at 14M, VV at 31M and 70M, AoA at 160M, and Random at 410M and 1B (for 1B, we compare only Random and VV). The pattern suggests that curriculum benefits are most pronounced when model capacity is constrained,

| Group | Ordering | ARC-E | ARC-C | PIQA | SciQ | LogiQA | Lambada | WinoGrande | WSC | Avg. |
|-------|-----------|-------------|-------------|-------------|-------------|-------------|-------------|-------------|-------------|-------------|
| 14M | Frequency | 32.7 | 17.2 | 55.9 | 51.0 | 21.5 | 10.2 | 50.4 | 62.8 | 37.7 |
| | AoA | 32.9 | 17.7 | 56.3 | 50.9 | 20.7 | 9.7 | 50.3 | 51.6 | 36.3 |
| | VV | 32.4 | 18.2 | 55.9 | 51.8 | 18.9 | 11.1 | 50.8 | 51.0 | 36.3 |
| | Random | 31.5 | 18.0 | 55.4 | 41.8 | 21.5 | 5.9 | 50.3 | 61.5 | 35.7 |
| 31M | Frequency | 35.0 | 16.9 | 56.9 | 59.0 | 21.3 | 17.6 | 50.3 | 39.4 | 37.0 |
| | AoA | 34.4 | 18.0 | 57.6 | 53.5 | 22.1 | 13.8 | 50.1 | 46.2 | 37.0 |
| | VV | 35.4 | 17.6 | 56.3 | 58.4 | 20.7 | 16.4 | 52.1 | 59.6 | 39.6 |
| | Random | 34.5 | 17.6 | 57.3 | 52.1 | 21.1 | 13.3 | 50.1 | 50.6 | 37.1 |
| 70M | Frequency | 39.4 | 19.0 | 59.3 | 67.0 | 21.0 | 20.7 | 50.2 | 36.5 | 39.2 |
| | AoA | 39.5 | 18.3 | 58.9 | 68.7 | 20.6 | 23.6 | 50.4 | 36.5 | 39.6 |
| | VV | 41.7 | 17.3 | 59.6 | 73.6 | 21.4 | 27.3 | 50.7 | 37.5 | 41.1 |
| | Random | 38.1 | 17.7 | 59.7 | 64.5 | 23.3 | 20.4 | 52.3 | 35.9 | 39.0 |
| 160M | Frequency | 47.2 | 17.9 | 63.3 | 77.3 | 20.4 | 40.9 | 53.0 | 36.5 | 44.6 |
| | AoA | 44.9 | 20.0 | 62.8 | 77.4 | 21.5 | 38.3 | 52.6 | 43.3 | 45.1 |
| | VV | 46.1 | 18.6 | 63.7 | 76.4 | 20.3 | 38.2 | 50.2 | 45.2 | 44.8 |
| | Random | 43.9 | 19.2 | 62.3 | 73.7 | 18.4 | 32.9 | 50.4 | 36.5 | 42.2 |
| 410M | Frequency | 50.2 | 21.5 | 66.5 | 82.5 | 23.2 | 50.9 | 51.9 | 36.5 | 47.9 |
| | AoA | 51.7 | 21.4 | 66.5 | 80.5 | 21.2 | 50.9 | 51.1 | 36.5 | 47.5 |
| | VV | 50.8 | 21.0 | 67.5 | 82.0 | 21.8 | 50.5 | 53.2 | 36.5 | 47.9 |
| | Random | 51.9 | 21.2 | 66.8 | 80.9 | 21.7 | 51.5 | 53.4 | 60.6 | 51.0 |
| 1B | VV | 55.3 | 23.7 | 69.6 | 85.3 | 21.2 | 55.1 | 53.7 | 36.5 | 50.1 |
| | Random | 56.9 | 24.3 | 70.7 | 84.0 | 22.1 | 56.2 | 53.4 | 36.5 | 50.5 |

Table 1. Zero-shot performance by data ordering (Frequency, Age-of-Acquisition, VV, Random). At 1B, results are reported only for VV and Random.

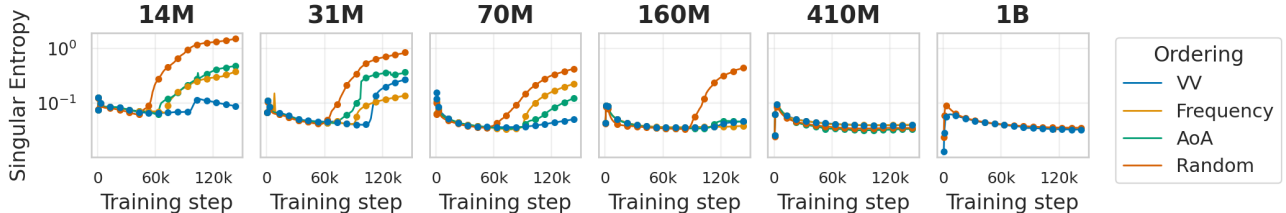


Figure 2. Singular entropy of the language modeling head versus training step. For models up to 160M parameters, Random ordering produces sharp late-stage increases in singular entropy, indicating collapse toward a spiked spectrum associated with saturation. Curriculum-based orderings maintain lower entropy, avoiding the degenerate spectral regime associated with performance degradation.

consistent with our saturation hypothesis.

Ordering effects can be heterogeneous across capabilities

Aggregate benchmark averages (Table 1) can mask targeted changes on individual capabilities. Using BLiMP probes at 300B tokens, we observe ordering-dependent differences that are concentrated in a small number of syntactic phenomena rather than spread uniformly across probes. Across 14M–410M models, the Verb Variation curriculum (VV) improves *wh*-questions object-gap accuracy by ≈ 9 percentage points on average at the end of training, and improves causatives by ≈ 4 – 5 points (Appendix B). In contrast, the Frequency curriculum underperforms Random on superlative quantifiers by ≈ 14 points on average, with additional drops on ellipsis-N-bar (≈ 3 points) and only-NPI scope (≈ 4 points). Notably, Age-of-Acquisition shows no consis-

tent BLiMP advantages or regressions relative to Random under our thresholds, suggesting these effects are ordering-specific rather than a general consequence of non-random data presentation. At 1B, where only VV and Random were evaluated, the scale-dependent pattern in Table 1 suggests that VV advantages on specific syntactic constructions would similarly diminish, consistent with the narrowing curriculum effects observed at larger model scales.

These probe-level differences align with text characteristics (§4.1). VV explicitly prioritizes samples with higher verb diversity, which increases early exposure to varied predicate–argument structures and clause-level dependencies; this may support generalization on filler-gap constructions (*wh*-movement) and argument-structure alternations (causatives). Frequency, by contrast, places low-frequency, highly structured content (e.g., code and templated text)

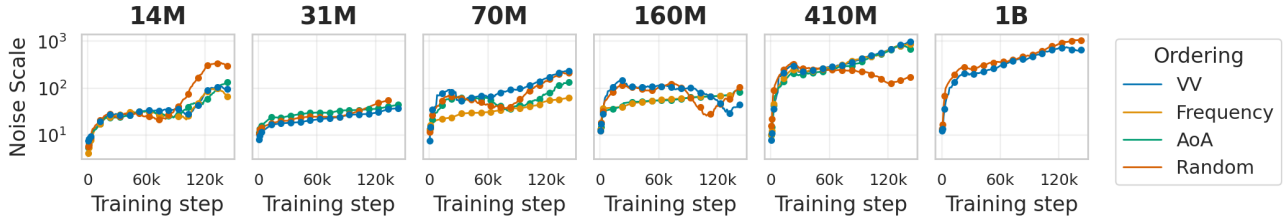


Figure 3. Gradient noise scale (GNS) versus training step across model sizes and orderings. Random ordering tends to produce higher GNS for smaller models (14M–70M), indicating noisier gradient estimates and less efficient optimization. At larger scales (160M–410M), the gap between Random and the curricula is smaller and less consistent.

early in training; while this can improve predictability, it reduces early exposure to the natural-language contexts that most strongly evidence quantifier scope and NPI licensing patterns. The result is that Frequency’s Table 1 performance can appear comparable to Random at aggregate level while underperforming on specific syntactic constructions. Appendix B provides the full data and visualizes these trajectories.

Curricula reduce gradient noise scale and singular entropy in smaller models Curriculum-based orderings reduce gradient noise scale (GNS) for smaller models, consistent with our theoretical predictions (§3). Figure 3 shows that for models at 14M–70M scale, Random ordering often exhibits higher GNS than curriculum-based orderings, particularly in later training phases. This pattern is consistent with the prediction that uniform sampling elevates gradient variance as training progresses. Higher GNS under Random ordering indicates noisier gradient estimates (McCandlish et al., 2018), which degrades optimization efficiency and can contribute to late-phase instability. At larger scales (160M–410M), the GNS differences between orderings are smaller and less consistent.

Random ordering also produces sharp late-stage increases in singular entropy for models up to 160M parameters (Figure 2), indicating collapse toward a spiked singular value distribution—a signature of spectral degeneration associated with saturation (Godey et al., 2024). Curriculum-based orderings maintain lower singular entropy throughout training, avoiding this collapse. The 410M model shows minimal entropy differences across orderings, consistent with the prediction that reduced gradient variance under curricula matters most when model capacity is constrained.

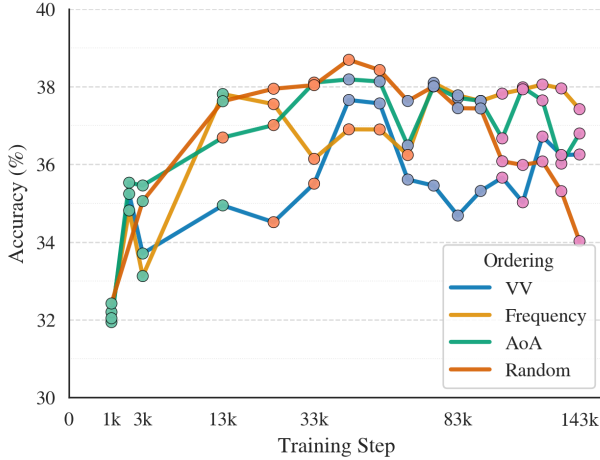
Shared phases; within-phase exposure drives stability For the 14M model, a single HMM trained jointly over trajectories from Age-of-Acquisition, Frequency, Verb Variation, and Random yields a shared set of latent training phases (Figure 4). This mirrors the finding of van der Wal et al. (2025) that Pythia pretraining proceeds through consistent phases across random seeds when training the same

architecture on the same underlying corpus. In our setting, we hold the architecture, optimizer configuration, and data source fixed and change only the ordering; the shared transition map across orderings indicates that curricula do not create new phases, but change how training time and data exposure are allocated within shared phases.

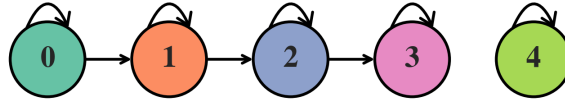
van der Wal et al. (2025) interpret these phases in terms of broader training phenomena: an early learning phase (roughly 10^3 – 10^4 steps) where representations change rapidly and linguistic information begins to be encoded, followed by a critical learning phase (roughly 10^4 – 10^5 steps) in which most benchmark improvements occur and representations stabilize, and then a later regime in which progress slows and small models can exhibit saturation and instability. Under this view, our result that orderings share a transition structure but differ in time spent in each state suggests a concrete mechanism for curricula: they change which data is encountered during the early and critical phases and how long the model remains there, which in turn can affect late-phase stability. The optimization diagnostics support this: curricula reduce gradient noise scale and singular-entropy collapse in later training, mitigating instability that emerges after the critical phase and correlating with higher end-of-run accuracy at matched compute.

Curricula primarily affect within-phase dynamics rather than changing the set of phases. The shared transition map across orderings supports our view that curricula regulate the difficulty of data encountered within phases, improving late-phase stability (Theorem 3.2).

Implications for Curriculum Design The GNS and singular entropy results suggest that the primary benefit of curricula for smaller models lies in maintaining optimization stability rather than accelerating early learning. These results motivate several curriculum design variants. First, hybrid curricula could transition between orderings based on detected phase membership or spectral diagnostics—for instance, monitoring singular entropy to detect the onset of saturation and adjusting data difficulty accordingly. Second, since curricula affect within-phase data exposure rather than the phases themselves, phase-adaptive curricula could dy-



(a) Average accuracy by curriculum. Checkpoints are colored by the corresponding HMM state from (b).



(b) HMM state transition diagram.

Figure 4. Shared phases and within-phase dynamics for the 14M model. a shows the average accuracy trajectory for Random, Age-of-Acquisition, Frequency, and VV, with checkpoints colored by the HMM state from b. b shows the shared HMM state transition diagram learned jointly across orderings. Curricula do not change the phases, but affect the accuracy trajectory within those phases.

namically adjust the data ordering based on estimated phase membership (e.g., using lightweight online monitoring of the metrics in Table 9 or the GNS). Third, the observation that curriculum benefits are most pronounced for smaller models suggests that adaptive strategies could allocate more aggressive curricula to capacity-constrained regimes while relaxing constraints for larger models where the softmax bottleneck is less severe. These approaches could potentially achieve more robust improvements across diverse evaluation metrics than any single static ordering.

Beyond these adaptive strategies, the curricula studied here are attractive because they are inexpensive to compute and scale to large corpora. An immediate extension is to move from a fully sorted ordering to a small number of difficulty stages (k-stage curricula) that are easier to implement in distributed pipelines. More broadly, modern pretraining mixtures are heterogeneous; difficulty scores that account for domain or mixture composition (Xie et al., 2023), as well as multilingual and modality-aware scores, are necessary for deploying these ideas beyond English-centric lexical resources.

6. Conclusion

We analyzed how pretraining data order affects LLM learning dynamics and stability. Using Pythia models, we combined HMM-based phase analysis with gradient noise scale and singular entropy diagnostics to compare three curricula—Age-of-Acquisition, word frequency, and Verb Variation (VV)—against Random ordering.

The joint HMM analysis (Figure 4) confirms that all orderings share latent training phases; differences arise from which data appears within these phases. For smaller models (14M–70M), Random ordering produces higher gradient noise scale; for models up to 160M parameters, Random ordering also produces higher singular entropy, corresponding to noisier optimization and a late-stage collapse toward a spiked spectrum in the language modeling head. Curriculum-based orderings reduce both quantities and are associated with less late-phase degradation consistent with softmax-bottleneck saturation (Godey et al., 2024; Michaelov & Bergen, 2023). At larger scales, the gaps in gradient noise scale and singular entropy narrow and curriculum gains shrink. Downstream accuracy varies by scale, with different orderings attaining the best average score for different model sizes (Table 1).

Our theoretical framework (Theorem 3.2) formalizes a mechanism linking difficulty pacing to optimization stability: by controlling the variance of stochastic gradients through structured data exposure, curricula can maintain tighter stability bounds than uniform sampling. The empirical results support this view—curricula reduce gradient noise scale and singular entropy in smaller models, and these reductions coincide with improved late-phase accuracy. This suggests a practical guideline: curricula are most valuable when model capacity is constrained and late-stage saturation is a concern; at larger scales where capacity suffices, random ordering performs comparably.

Three limitations suggest directions for future work. First, our analysis assumes a fixed set of 2048-token training sequences; relaxing this assumption suggests making sequence packing/chunking and document grouping themselves difficulty-aware, rather than only scoring and ordering a predetermined sample set. Second, it remains unclear how strongly the phase-conditional stability effects observed here transfer to substantially larger model scales and to alternative datasets and curriculum strategies. Third, the probe-level BLiMP results (§5) show that orderings can have heterogeneous effects across syntactic phenomena; identifying which linguistic structures benefit from which orderings would enable more targeted curriculum design. Our findings show that data ordering shapes within-phase optimization with measurable effects on final model quality.

Impact Statement

This work studies how pretraining data ordering affects learning dynamics and stability in language models. A potential positive impact is improved training efficiency and robustness at fixed compute budgets: for smaller, capacity-constrained models, curricula that reduce gradient noise and mitigate softmax-bottleneck saturation can improve end-of-run performance at matched compute.

Potential negative impacts are indirect. Improved training efficiency can lower barriers to training capable models, including by actors who may deploy them irresponsibly. Curricula also change content exposure over training and can amplify dataset biases or reduce coverage if difficulty scores systematically prioritize or deprioritize particular domains, languages, or modalities. We use publicly available training data (The Pile) under the dataset’s licenses; while we do not perform targeted processing of personally identifiable information, large-scale web corpora may contain incidental PII.

References

Bengio, Y., Louradour, J., Collobert, R., and Weston, J. Curriculum learning. In *Proceedings of the 26th Annual International Conference on Machine Learning*. ACM, 2009.

Biderman, S., Schoelkopf, H., Anthony, Q. G., Bradley, H., O’Brien, K., Hallahan, E., Khan, M. A., Purohit, S., Prashanth, U. S., Raff, E., et al. Pythia: A suite for analyzing large language models across training and scaling. In *International Conference on Machine Learning*, pp. 2397–2430. PMLR, 2023.

Bisk, Y., Zellers, R., Gao, J., Choi, Y., et al. Piqa: Reasoning about physical commonsense in natural language. In *Proceedings of the AAAI conference on artificial intelligence*, volume 34, pp. 7432–7439, 2020.

Bottou, L., Curtis, F. E., and Nocedal, J. Optimization methods for large-scale machine learning. *SIAM review*, 60(2):223–311, 2018.

Brysbaert, M. and New, B. SUBTLEX-US: A large-scale word frequency database for American English. *Behavior research methods*, 41(4):977–984, 2009.

Campos, D. Curriculum learning for language modeling. *arXiv preprint arXiv:2108.02170*, 2021.

Chai, Y., Liu, Q., Wang, S., Sun, Y., Peng, Q., and Wu, H. On training data influence of gpt models. In *Proceedings of the 2024 Conference on Empirical Methods in Natural Language Processing*, pp. 3126–3150, 2024.

Clark, P., Cowhey, I., Etzioni, O., Khot, T., Sabharwal, A., Schoenick, C., and Tafjord, O. Think you have solved question answering? try arc, the ai2 reasoning challenge. *arXiv preprint arXiv:1803.05457*, 2018.

Cornacchia, E. and Mossel, E. A mathematical model for curriculum learning for parities. In Krause, A., Brunskill, E., Cho, K., Engelhardt, B., Sabato, S., and Scarlett, J. (eds.), *Proceedings of the 40th International Conference on Machine Learning*, volume 202 of *Proceedings of Machine Learning Research*, pp. 6402–6423. PMLR, 23–29 Jul 2023. URL <https://proceedings.mlr.press/v202/cornacchia23a.html>.

Elman, J. L. Learning and development in neural networks: The importance of starting small. *Cognition*, 48(1):71–99, 1993.

Fan, S. and Jaggi, M. Irreducible curriculum for language model pretraining. *CoRR*, 2023.

Gao, L., Biderman, S., Black, S., Golding, L., Hoppe, T., Foster, C., Phang, J., He, H., Thite, A., Nabeshima, N., et al. The pile: An 800gb dataset of diverse text for language modeling. *arXiv preprint arXiv:2101.00027*, 2020.

Garrigos, G. and Gower, R. M. Handbook of convergence theorems for (stochastic) gradient methods. *arXiv preprint arXiv:2301.11235*, 2023.

Godey, N., de la Clergerie, É. V., and Sagot, B. Why do small language models underperform? studying language model saturation via the softmax bottleneck. In *First Conference on Language Modeling*, 2024. URL <https://openreview.net/forum?id=MoitXW1XcS>.

Guiraud, P. *Problèmes et méthodes de la statistique linguistique*. Synthese Library. Springer Netherlands, 1960. ISBN 9789027700254. URL <https://books.google.com/books?id=CLGgbATDcG8C>.

Guu, K., Webson, A., Pavlick, E., Dixon, L., Tenney, I., and Bolukbasi, T. Simfluence: Modeling the influence of individual training examples by simulating training runs. *arXiv preprint arXiv:2303.08114*, 2023.

Hacohen, G. and Weinshall, D. On the power of curriculum learning in training deep networks. In Chaudhuri, K. and Salakhutdinov, R. (eds.), *Proceedings of the 36th International Conference on Machine Learning*, volume 97 of *Proceedings of Machine Learning Research*, pp. 2535–2544. PMLR, 09–15 Jun 2019. URL <https://proceedings.mlr.press/v97/hacohen19a.html>.

Hoffmann, J., Borgeaud, S., Mensch, A., Buchatskaya, E., Cai, T., Rutherford, E., de Las Casas, D., Hendricks, L. A., Welbl, J., Clark, A., et al. Training compute-optimal large language models. In *Proceedings of the 36th International Conference on Neural Information Processing Systems*, pp. 30016–30030, 2022.

Hu, M. Y., Chen, A., Saphra, N., and Cho, K. Delays, detours, and forks in the road: Latent state models of training dynamics. *Transactions on Machine Learning Research*, 2023, 2023.

Kaplan, J., McCandlish, S., Henighan, T., Brown, T. B., Chess, B., Child, R., Gray, S., Radford, A., Wu, J., and Amodei, D. Scaling laws for neural language models. *arXiv preprint arXiv:2001.08361*, 2020.

Koh, P. W. and Liang, P. Understanding black-box predictions via influence functions. In *International conference on machine learning*, pp. 1885–1894. PMLR, 2017.

Komatsuzaki, A. One epoch is all you need. *arXiv preprint arXiv:1906.06669*, 2019.

Kong, Y., Liu, L., Wang, J., and Tao, D. Adaptive curriculum learning. In *Proceedings of the IEEE/CVF International Conference on Computer Vision (ICCV)*, pp. 5067–5076, October 2021.

Kuperman, V., Stadthagen-Gonzalez, H., and Brysbaert, M. Age-of-acquisition ratings for 30,000 english words. *Behavior research methods*, 44(4):978–990, 2012.

Lee, B. W. and Lee, J. LFTK: Handcrafted features in computational linguistics. In Kochmar, E., Burstein, J., Horbach, A., Laermann-Quante, R., Madnani, N., Tack, A., Yaneva, V., Yuan, Z., and Zesch, T. (eds.), *Proceedings of the 18th Workshop on Innovative Use of NLP for Building Educational Applications (BEA 2023)*, pp. 1–19, Toronto, Canada, July 2023. Association for Computational Linguistics. doi: 10.18653/v1/2023.bea-1.1. URL <https://aclanthology.org/2023.bea-1.1/>.

Levesque, H. J., Davis, E., and Morgenstern, L. The winograd schema challenge. *KR*, 2012:13th, 2012.

Li, C., Zhang, M., and He, Y. The stability-efficiency dilemma: Investigating sequence length warmup for training gpt models. *Advances in Neural Information Processing Systems*, 35:26736–26750, 2022.

Liu, J., Cui, L., Liu, H., Huang, D., Wang, Y., and Zhang, Y. Logiqa: A challenge dataset for machine reading comprehension with logical reasoning. *arXiv preprint arXiv:2007.08124*, 2020.

McCandlish, S., Kaplan, J., Amodei, D., and OpenAI Dota Team. An empirical model of large-batch training. *arXiv preprint arXiv:1812.06162*, 2018.

Michaelov, J. and Bergen, B. Emergent inabilities? inverse scaling over the course of pretraining. In Bouamor, H., Pino, J., and Bali, K. (eds.), *Findings of the Association for Computational Linguistics: EMNLP 2023*, pp. 14607–14615, Singapore, December 2023. Association for Computational Linguistics. doi: 10.18653/v1/2023.findings-emnlp.973. URL <https://aclanthology.org/2023.findings-emnlp.973/>.

Nagatsuka, K., Broni-Bediako, C., and Atsumi, M. Length-based curriculum learning for efficient pre-training of language models. *New Generation Computing*, 41(1):109–134, 2023.

Paperno, D., Kruszewski, G., Lazaridou, A., Pham, Q. N., Bernardi, R., Pezzelle, S., Baroni, M., Boleda, G., and Fernández, R. The lambada dataset: Word prediction requiring a broad discourse context. *arXiv preprint arXiv:1606.06031*, 2016.

Pruthi, G., Liu, F., Kale, S., and Sundararajan, M. Estimating training data influence by tracing gradient descent. *Advances in Neural Information Processing Systems*, 33:19920–19930, 2020.

Raffel, C., Shazeer, N., Roberts, A., Lee, K., Narang, S., Matena, M., Zhou, Y., Li, W., and Liu, P. J. Exploring the limits of transfer learning with a unified text-to-text transformer. *Journal of machine learning research*, 21(140):1–67, 2020.

Sakaguchi, K., Bras, R. L., Bhagavatula, C., and Choi, Y. Winogrande: An adversarial winograd schema challenge at scale. *Communications of the ACM*, 64(9):99–106, 2021.

van der Wal, O., Lesci, P., Müller-Eberstein, M., Saphra, N., Schoelkopf, H., Zuidema, W., and Biderman, S. Polypythias: Stability and outliers across fifty language model pre-training runs. In *The Thirteenth International Conference on Learning Representations*, 2025. URL <https://openreview.net/forum?id=bmrYu2Ekdz>.

Van Heuven, W. J., Mandera, P., Keuleers, E., and Brysbaert, M. Subtlex-uk: A new and improved word frequency database for british english. *Quarterly journal of experimental psychology*, 67(6):1176–1190, 2014.

Weinshall, D., Cohen, G., and Amir, D. Curriculum learning by transfer learning: Theory and experiments with deep networks. In *International conference on machine learning*, pp. 5238–5246. PMLR, 2018.

Welbl, J., Liu, N. F., and Gardner, M. Crowdsourcing multiple choice science questions. *arXiv preprint arXiv:1707.06209*, 2017.

Xie, S. M., Pham, H., Dong, X., Du, N., Liu, H., Lu, Y.,
Liang, P. S., Le, Q. V., Ma, T., and Yu, A. W. Doremi:
Optimizing data mixtures speeds up language model pre-
training. *Advances in Neural Information Processing
Systems*, 36:69798–69818, 2023.

Zhou, T. and Bilmes, J. Minimax curriculum learning: Ma-
chine teaching with desirable difficulties and scheduled
diversity. In *International conference on learning repre-
sentations*, 2018.

A. Theoretical Framework: Additional Details and Proofs

A.1. Softmax bottleneck and singular entropy

We state the formal lemma and define the diagnostic used in §3.

The saturation problem follows [Godey et al. \(2024\)](#). Let r denote the dimension of the final-layer representation (equivalently, an upper bound on the rank of the output head). The final linear layer maps an r -dimensional representation to a distribution over a vocabulary of size V , which can be viewed as learning a low-rank approximation $W_r \in \mathbb{R}^{V \times r}$ of a theoretically optimal, high-rank matrix W^* .

Lemma A.1 (Inherent Performance Gap, from [Godey et al. \(2024\)](#)). *Let W^* be the optimal language modeling head, with singular values $\{\sigma_i\}_{i=1}^V$. Any model with a linear head of rank at most r incurs a minimal loss gap, where the approximation error is lower-bounded by the discarded spectral energy:*

$$\min_{\text{rank}(W_r) \leq r} \|W_r - W^*\|_F^2 = \sum_{i=r+1}^V \sigma_i^2 \quad (3)$$

When r is small relative to the intrinsic rank of W^* , this gap can be substantial, leading to performance saturation.

To quantify the spectral structure of the language modeling head during training, we use singular entropy as a diagnostic ([Godey et al., 2024](#)). Let $\{\sigma_i\}_{i=1}^r$ denote the singular values of the head matrix W , normalized to form a probability distribution $p_i = \sigma_i / \sum_j \sigma_j$. The singular entropy is defined as the Kullback-Leibler divergence between this distribution and the uniform distribution:

$$H_{\text{sing}}(W) = D_{\text{KL}}(p \parallel \mathcal{U}) = \sum_{i=1}^r p_i \log(r \cdot p_i), \quad (4)$$

where \mathcal{U} is the uniform distribution over r components. Note that $H_{\text{sing}}(W) = \log r - H(p)$, where $H(p) = -\sum_i p_i \log p_i$ is the Shannon entropy of p ; thus H_{sing} measures divergence from the maximum-entropy (uniform) spectrum and equals 0 when p is uniform. Low singular entropy corresponds to a more uniform distribution of singular values; high singular entropy corresponds to a more concentrated (spiked) spectrum. [Godey et al. \(2024\)](#) associate these spectral regimes with saturation dynamics.

A.2. Ideal difficulty and gradient variance

We state the formal assumption used in §3.

Assumption A.2 (Ideal Difficulty and Gradient Variance). Consider SGD updates of the form (1) and define the stochastic gradient noise

$$\xi_t = g_t - \mathbb{E}[g_t \mid \theta_t], \quad \sigma_t^2 = \mathbb{E}[\|\xi_t\|_2^2 \mid \theta_t].$$

There exist constants σ_{easy}^2 and σ_{hard}^2 and a neighborhood $\mathcal{N}(\theta^*)$ such that

$$\sup_{\theta \in \mathcal{N}(\theta^*)} \mathbb{E}_{z \sim \mathcal{P}_{\text{easy}}} [\|\nabla \ell(\theta, z) - \nabla F_{\text{easy}}(\theta)\|_2^2] \leq \sigma_{\text{easy}}^2,$$

$$\inf_{\theta \in \mathcal{N}(\theta^*)} \mathbb{E}_{z \sim \mathcal{P}_{\text{hard}}} [\|\nabla \ell(\theta, z) - \nabla F_{\text{hard}}(\theta)\|_2^2] \geq \sigma_{\text{hard}}^2,$$

with $\sigma_{\text{hard}}^2 > \sigma_{\text{easy}}^2$, where F_{easy} and F_{hard} denote the population risks restricted to $\mathcal{P}_{\text{easy}}$ and $\mathcal{P}_{\text{hard}}$, respectively.

A.3. Uniform-sampling variance dynamics and difficulty pacing

We give the formal details underlying §3.

Effective gradient variance under uniform sampling. To formalize the notion of “effective” gradient variance, consider uniform sampling from the full data distribution \mathcal{P} and write it as a mixture of easy and hard components,

$$\mathcal{P} = (1 - \rho) \mathcal{P}_{\text{easy}} + \rho \mathcal{P}_{\text{hard}}, \quad \rho \in (0, 1).$$

At training time t , let $\alpha_t \in [0, 1]$ denote the fraction of the stochastic gradient contribution attributable to easy examples, so that the conditional gradient-noise variance can be decomposed as

$$\sigma_t^2 = \alpha_t \sigma_{\text{easy}}^2 + (1 - \alpha_t) \sigma_{\text{hard}}^2 + \Delta_t,$$

where Δ_t collects covariance terms between easy and hard contributions.

Assumption A.3 (Dynamic Increase of Effective Gradient Variance). Under uniform sampling from \mathcal{P} , training proceeds so that α_t decreases over time: as the model fits the easy subset $\mathcal{D}_{\text{easy}}$, the corresponding gradients vanish and the stochastic gradient g_t becomes dominated by contributions from $\mathcal{D}_{\text{hard}}$. Consequently, the effective gradient variance σ_t^2 transitions from a regime close to σ_{easy}^2 to a regime close to σ_{hard}^2 , and the GNS increases correspondingly.

Pacing of difficulty. To connect the stability analysis to concrete curricula, it is useful to model explicitly how data ordering is induced by a difficulty score and a pacing function. Let d be a scalar difficulty function on training samples, and let $D = \{z_i\}_{i=1}^N$ denote the training dataset sorted in non-decreasing order of $d(z_i)$. Training progress is parameterized by $t \in [0, 1]$, representing the fraction of total training steps.

Definition A.4 (Pacing Function). Given a difficulty score d , a pacing function is a mapping $p: [0, 1] \rightarrow \mathbb{R}$ that specifies the maximal difficulty level exposed at training progress t . The subset of training data available at time t is

$$D_t = \{z_i \in D \mid d(z_i) \leq p(t)\}.$$

Let d_{\min} and d_{\max} denote the minimum and maximum values of d over D . A linear pacing function sets $p(t) = d_{\min} + t(d_{\max} - d_{\min})$ and exposes the full difficulty range at a constant rate over training. Concave schedules, such as $p(t) = d_{\min} + \sqrt{t}(d_{\max} - d_{\min})$, allocate more training updates to easier samples by prolonging the period in which D_t contains predominantly low-difficulty examples. Convex schedules, such as $p(t) = d_{\min} + t^2(d_{\max} - d_{\min})$, introduce harder samples more aggressively by expanding D_t toward high-difficulty regions early in training.

A.4. Full statement of Theorem 3.2

Theorem A.5 (Theorem 3.2, restatement). *Given a difficulty score d and pacing function $p: [0, 1] \rightarrow \mathbb{R}$, let a curriculum present training samples in order of increasing d according to $p(t)$, so that the sampling distribution \mathcal{P}_t at (rescaled) time t interpolates between the easy distribution $\mathcal{P}_{\text{easy}}$ and the full data distribution \mathcal{P} . Assume that F is μ -strongly convex with L -Lipschitz gradient and that Assumptions A.2–A.3 hold. For SGD with constant step size $\eta \in (0, 1/L]$:*

1. *There exists a stability threshold*

$$\sigma_{\text{stab}}^2(R) = \frac{\mu}{\eta} R^2,$$

parameterized by a target radius $R > 0$, such that any sampling scheme whose effective gradient variance satisfies $\sup_t \sigma_t^2 \leq \sigma_{\text{stab}}^2(R)$ and initialization satisfies $\|\theta_0 - \theta^\|_2^2 \leq R^2$ guarantees*

$$\sup_t \mathbb{E}[\|\theta_t - \theta^*\|_2^2] \leq R^2.$$

2. *Under uniform sampling from \mathcal{P} , the effective gradient variance σ_t^2 eventually approaches σ_{hard}^2 by Assumption A.3. If $\sigma_{\text{hard}}^2 > \sigma_{\text{stab}}^2(R)$, then the best bound obtainable from Theorem A.6 has R replaced by*

$$R_{\text{unif}}^2 = \frac{\eta}{\mu} \sigma_{\text{hard}}^2 > R^2.$$

3. *For a curriculum induced by (d, p) , early iterations sample predominantly from $\mathcal{P}_{\text{easy}}$ and thus operate in a regime where the effective variance is close to σ_{easy}^2 . As $p(t)$ increases, harder examples are introduced gradually; if the pacing is chosen so that the resulting effective variance stays below $\sigma_{\text{stab}}^2(R)$ over an initial horizon $t \leq T_{\text{stab}}$, Theorem A.6 implies*

$$\sup_{t \leq T_{\text{stab}}} \mathbb{E}[\|\theta_t - \theta^*\|_2^2] \leq R^2.$$

A.5. SGD Stability Lemma

Lemma A.6 (SGD Stability under Bounded Gradient Variance). *Assume that F is μ -strongly convex and has L -Lipschitz gradient, and consider SGD updates of the form (1) with constant step size $\eta \in (0, 1/L]$. Suppose that for all t ,*

$$\mathbb{E}[g_t \mid \theta_t] = \nabla F(\theta_t) \quad \text{and} \quad \mathbb{E}[\|g_t - \nabla F(\theta_t)\|_2^2 \mid \theta_t] \leq \sigma^2.$$

Then the iterates satisfy

$$\begin{aligned} \mathbb{E}[\|\theta_t - \theta^*\|_2^2] &\leq (1 - \mu\eta)^t \|\theta_0 - \theta^*\|_2^2 \\ &\quad + \left(1 - (1 - \mu\eta)^t\right) \frac{\eta}{\mu} \sigma^2, \quad t \geq 0. \end{aligned} \quad (5)$$

where θ^ is the unique minimizer of F .*

A.6. Proofs for Theorems A.6 and 3.2

Proof of Theorem A.6. The proof follows standard SGD analysis. Taking conditional expectation given θ_t ,

$$\begin{aligned} \mathbb{E}[\|\theta_{t+1} - \theta^*\|_2^2 \mid \theta_t] &= \mathbb{E}[\|\theta_t - \theta^* - \eta g_t\|_2^2 \mid \theta_t] \\ &= \|\theta_t - \theta^* - \eta \nabla F(\theta_t)\|_2^2 \\ &\quad + \eta^2 \mathbb{E}[\|g_t - \nabla F(\theta_t)\|_2^2 \mid \theta_t], \end{aligned}$$

since the mixed term has zero conditional expectation under $\mathbb{E}[g_t \mid \theta_t] = \nabla F(\theta_t)$. For μ -strongly convex F with L -Lipschitz gradient and $\eta \in (0, 1/L]$, a standard contraction bound gives

$$\|\theta_t - \theta^* - \eta \nabla F(\theta_t)\|_2^2 \leq (1 - \mu\eta) \|\theta_t - \theta^*\|_2^2 \quad \text{for all } t$$

(see, e.g., (Bottou et al., 2018)). Combining with the variance bound yields

$$\mathbb{E}[\|\theta_{t+1} - \theta^*\|_2^2 \mid \theta_t] \leq (1 - \mu\eta) \|\theta_t - \theta^*\|_2^2 + \eta^2 \sigma^2.$$

Taking unconditional expectation and unrolling the recursion gives (5). \square

Proof of Theorem 3.2. For any sampling scheme with $\sup_t \sigma_t^2 \leq \bar{\sigma}^2$, Theorem A.6 gives

$$\mathbb{E}[\|\theta_t - \theta^*\|_2^2] \leq (1 - \mu\eta)^t \|\theta_0 - \theta^*\|_2^2 + \left(1 - (1 - \mu\eta)^t\right) \frac{\eta}{\mu} \bar{\sigma}^2,$$

Choosing $\bar{\sigma}^2 = \sigma_{\text{stab}}^2(R) = \frac{\mu}{\eta} R^2$ and assuming $\|\theta_0 - \theta^*\|_2^2 \leq R^2$, the right-hand side is a convex combination of two quantities each at most R^2 , yielding the claim in part (1).

For part (2), Assumption A.3 implies that under uniform sampling the effective variance approaches σ_{hard}^2 , so $\bar{\sigma}^2$ in the bound of Theorem A.6 must be taken at least as large as σ_{hard}^2 . The corresponding asymptotic radius is then $R_{\text{unif}}^2 = (\eta/\mu)\sigma_{\text{hard}}^2$, which exceeds R^2 when $\sigma_{\text{hard}}^2 > \sigma_{\text{stab}}^2(R)$.

For part (3), curricula induced by (d, p) define a family of intermediate distributions \mathcal{P}_t whose support is contained in $\mathcal{D}_t = \{z_i \mid d(z_i) \leq p(t)\}$ and evolves from $\mathcal{D}_{\text{easy}}$ to the full dataset. By Assumption A.2, the effective variance when sampling from $\mathcal{P}_{\text{easy}}$ is close to σ_{easy}^2 , and gradual inclusion of hard samples through $p(t)$ can keep $\sup_{t \leq T_{\text{stab}}} \sigma_t^2$ below $\sigma_{\text{stab}}^2(R)$ over an initial horizon $t \leq T_{\text{stab}}$. Applying Theorem A.6 over this horizon with $\bar{\sigma}^2 = \sigma_{\text{stab}}^2(R)$ gives the stated bound. \square

B. Shuffle Ordering Effects on BLiMP Trajectories

This appendix analyzes shuffle-ordering effects on BLiMP trajectories at 300B tokens. We compare each ordering to Random across model sizes and focus on probes with consistent, non-negligible differences. Table 2 summarizes final accuracy for selected probes; Figure 5 shows pairwise training trajectories for the key comparisons.

| Probe | Ordering | 14M | 31M | 70M | 160M | 410M |
|-------------------------|-----------|-------------|-------------|-------------|-------------|-------------|
| wh-questions object-gap | VV | 54.6 | 74.2 | 77.5 | 76.2 | 82.2 |
| | AoA | 53.1 | 61.9 | 70.1 | 77.8 | 83.7 |
| | Frequency | 42.9 | 64.3 | 61.6 | 75.9 | 85.4 |
| | Random | 42.4 | 55.5 | 63.9 | 75.0 | 83.7 |
| Causative | VV | 66.5 | 66.5 | 73.9 | 73.8 | 78.3 |
| | AoA | 61.6 | 64.0 | 68.3 | 72.8 | 76.3 |
| | Frequency | 61.8 | 62.2 | 65.8 | 72.3 | 77.7 |
| | Random | 58.5 | 64.4 | 67.5 | 71.6 | 74.8 |
| Superlative quantifiers | VV | 31.4 | 47.4 | 71.5 | 77.6 | 86.6 |
| | AoA | 26.3 | 75.1 | 65.6 | 87.6 | 81.7 |
| | Frequency | 35.5 | 62.6 | 43.8 | 80.5 | 89.1 |
| | Random | 61.9 | 63.1 | 75.5 | 95.3 | 85.6 |
| Only-NPI scope | VV | 58.7 | 67.6 | 48.8 | 76.6 | 70.9 |
| | AoA | 50.4 | 56.5 | 67.2 | 61.7 | 76.0 |
| | Frequency | 58.9 | 70.0 | 26.6 | 71.7 | 64.0 |
| | Random | 61.3 | 58.0 | 60.8 | 54.4 | 78.7 |
| Ellipsis N-bar | VV | 61.4 | 69.5 | 72.8 | 83.7 | 85.3 |
| | AoA | 54.1 | 62.9 | 70.0 | 80.7 | 85.9 |
| | Frequency | 57.1 | 58.9 | 65.9 | 77.6 | 81.7 |
| | Random | 56.8 | 61.2 | 70.1 | 82.7 | 87.0 |

Table 2. Final BLiMP accuracy (%) at 300B tokens for selected probes. Best result per probe and model size in bold.

C. Five-shot Downstream Evaluation

We report five-shot downstream performance for the same evaluation suite as in the main paper. For each benchmark, we evaluate the final checkpoints after 300B tokens using a fixed five-shot prompting setup; Table 3 summarizes accuracy by ordering and model size. These results complement the zero-shot results in Table 1.

D. Computational Costs

Experiments on 14M and 31M models were conducted primarily using 64 2080Ti GPUs, while experiments on 70M, 160M, and 410M models were conducted using 16 80GB NVIDIA A100 GPUs. The computational cost in GPU-hours is provided in Table 4. We observe training times comparable to those in the original Pythia paper. For 70M, 160M, and 410M, Biderman et al. (2023) report 510, 1030, and 2540 GPU-hours, respectively.

E. Curriculum Design and Scoring Details

E.1. Sample Splitting and Concatenation

We follow the data processing methodology of Pythia (Biderman et al., 2023), which employs “sequence packing” (Raffel et al., 2020) to create a dataset of uniform-length training samples. Documents from The Pile are processed into fixed-size, 2048-token sequences. As illustrated in Figure 6, this process concatenates smaller documents and splits larger ones across multiple sequences to maximize computational efficiency.

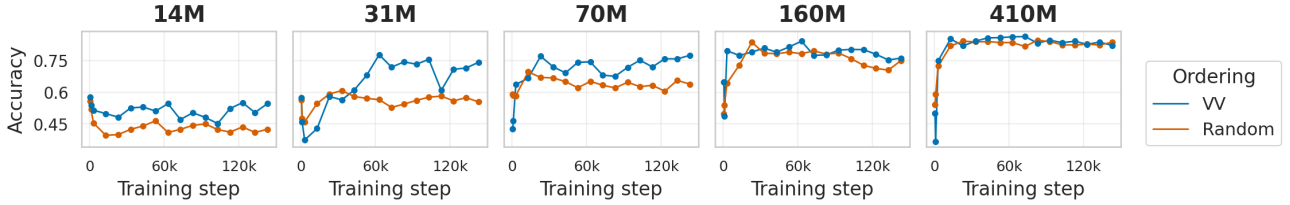
E.2. Scoring Functions

Since our chosen curriculum metrics are word-level, each 2048-token sample must first be detokenized to produce a word sequence before scoring. For a given detokenized text sequence S containing N words $\{w_1, \dots, w_N\}$, we define the difficulty scores as follows:

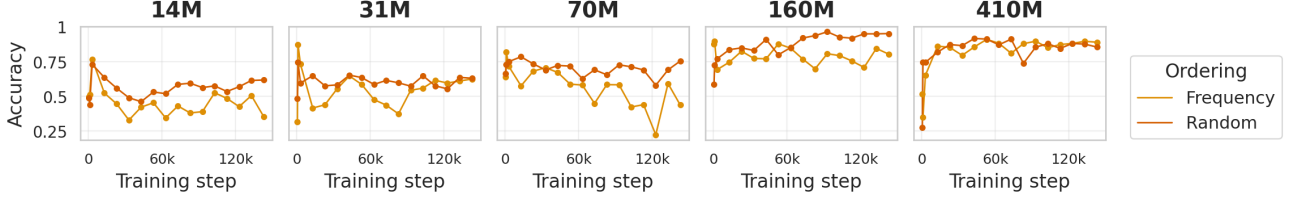
- **Age-of-Acquisition (AoA):** This score is based on the Kuperman et al. age of acquisition norms (Kuperman et al., 2012), representing the age at which a word is typically learned. The sequence score is the average AoA of its constituent words:

$$\text{Score}_{\text{AoA}}(S) = \frac{1}{N} \sum_{i=1}^N \text{AoA}(w_i)$$

- **Word Frequency (Freq):** This score is based on the SUBTLEX-US word frequency database (Brysbaert & New, 2009),



(a) VV vs Random on *wh*-questions object-gap. VV (blue) consistently outperforms Random (orange) at smaller scales.



(b) Frequency vs Random on superlative quantifiers. Random (orange) often outperforms Frequency (blue), with high variance across model sizes.

Figure 5. Pairwise ordering comparisons on BLiMP probes with consistent differences. These comparisons align with the effects discussed in the main text: VV improves *wh*-movement accuracy while Frequency can underperform Random on quantifier scope.

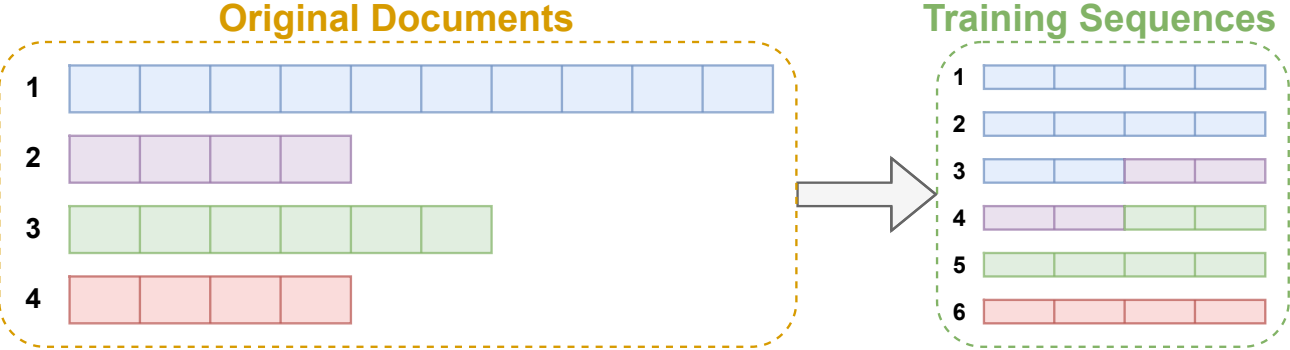


Figure 6. Illustration of the sequence packing process used by Pythia. Smaller documents are concatenated, while larger documents are split across multiple 2048-token samples.

using the Zipf scale (Van Heuven et al., 2014). The sequence score is the average Zipf value of its words:

$$\text{Score}_{\text{Freq}}(S) = \frac{1}{N} \sum_{i=1}^N \text{Zipf}(w_i)$$

- **Verb Variation (VV):** This score measures the linguistic diversity of verbs within a sample. It is computed as the number of unique verbs divided by the square root of the total number of verbs:

$$\text{Score}_{\text{VV}}(S) = \begin{cases} \frac{\text{Unique Verbs}}{\sqrt{\text{Total Verbs}}} & \text{if Total Verbs} \neq 0 \\ 0 & \text{if Total Verbs} = 0 \end{cases}$$

The square root adjustment helps ensure that the score more accurately reflects verb diversity rather than only sample length.

Normalizing by the number of words N mitigates length bias. For our curricula, we sort samples in ascending AoA, ascending Frequency (Zipf), and ascending VV; this corresponds to an easy-to-hard ordering, such that higher-score samples tend to have higher sample loss (Table 5). The linguistic features were computed using the LFTK toolkit (Lee & Lee, 2023), which relies on spaCy’s English pipeline (en_core_web_sm) and English lexical resources (Kuperman AoA; SUBTLEX

| Group | Ordering | ARC-E | ARC-C | PIQA | SciQ | LogiQA | Lambada | WinoGrande | WSC | Avg. |
|-------|-----------|-------------|-------------|-------------|-------------|-------------|-------------|-------------|-------------|-------------|
| 14M | Frequency | 31.6 | 17.1 | 55.6 | 47.9 | 23.7 | 5.7 | 50.2 | 36.5 | 33.6 |
| | AoA | 32.8 | 17.3 | 55.9 | 48.1 | 22.9 | 5.3 | 50.9 | 36.5 | 33.7 |
| | VV | 33.5 | 16.5 | 55.9 | 52.2 | 20.4 | 6.4 | 50.2 | 36.5 | 34.0 |
| | Random | 30.9 | 18.0 | 54.6 | 41.6 | 22.4 | 3.3 | 50.4 | 37.1 | 32.3 |
| 31M | Frequency | 35.6 | 17.3 | 57.2 | 56.3 | 23.4 | 10.9 | 49.1 | 36.5 | 35.8 |
| | AoA | 34.4 | 17.7 | 57.1 | 52.6 | 23.7 | 8.0 | 50.1 | 36.5 | 35.0 |
| | VV | 34.9 | 18.3 | 57.1 | 53.8 | 21.8 | 9.7 | 50.6 | 36.5 | 35.4 |
| | Random | 34.2 | 17.7 | 56.5 | 51.2 | 23.2 | 7.8 | 50.8 | 38.4 | 35.0 |
| 70M | Frequency | 38.1 | 17.3 | 60.3 | 65.8 | 22.7 | 15.1 | 50.6 | 36.5 | 38.3 |
| | AoA | 39.6 | 18.4 | 59.6 | 68.9 | 22.1 | 16.9 | 51.1 | 36.5 | 39.2 |
| | VV | 41.4 | 18.3 | 59.4 | 74.0 | 24.3 | 20.5 | 51.9 | 36.5 | 40.8 |
| | Random | 38.5 | 18.1 | 59.6 | 61.3 | 23.7 | 14.5 | 50.6 | 36.5 | 37.9 |
| 160M | Frequency | 47.1 | 18.4 | 64.0 | 83.5 | 20.3 | 33.3 | 51.5 | 36.5 | 44.3 |
| | AoA | 45.5 | 20.2 | 63.2 | 81.3 | 22.6 | 30.5 | 52.4 | 36.5 | 44.0 |
| | VV | 46.8 | 20.2 | 63.5 | 82.6 | 21.2 | 30.0 | 50.9 | 36.5 | 44.0 |
| | Random | 44.9 | 18.9 | 61.7 | 77.3 | 22.6 | 25.5 | 52.3 | 36.5 | 42.5 |
| 410M | Frequency | 53.7 | 23.0 | 67.3 | 89.3 | 23.7 | 45.0 | 51.6 | 36.5 | 48.8 |
| | AoA | 52.3 | 23.0 | 66.8 | 86.7 | 22.4 | 43.7 | 52.3 | 36.5 | 48.0 |
| | VV | 54.0 | 22.2 | 68.9 | 89.5 | 22.9 | 45.0 | 52.4 | 36.5 | 48.9 |
| | Random | 55.6 | 22.4 | 67.8 | 89.1 | 22.7 | 45.5 | 53.4 | 36.5 | 49.0 |
| 1B | VV | 58.2 | 24.1 | 69.6 | 90.0 | 24.7 | 49.3 | 52.3 | 36.5 | 50.6 |
| | Random | 59.6 | 25.9 | 70.5 | 92.0 | 23.0 | 50.6 | 53.4 | 36.5 | 51.4 |

Table 3. Five-shot performance by data ordering (Frequency, Age-of-Acquisition, VV, Random). At 1B, results are reported only for VV and Random due to compute constraints. Best result per group and metric is in bold.

| Model | A100 | 2080 Ti |
|-------|------|---------|
| 14M | 320 | 860 |
| 31M | 350 | 1170 |
| 70M | 530 | — |
| 160M | 1140 | — |
| 410M | 2730 | — |
| 1B | 5700 | — |

Table 4. Computational costs (in GPU-hours) for pretraining.

Zipf). Because The Pile contains code, numeric tables, and non-English text, some tokens fall outside these lexical resources and receive default values in the toolkit, which can affect the extreme low-score tails. We find the resulting scores remain strongly correlated with sample loss across model sizes (Table 5).

E.3. Correlation with Sample Loss

We computed the Pearson correlation between our sample scores (Average AoA, Average Word Frequency, and VV) and the average sample loss, measured across multiple checkpoints during training. As summarized in Table 5, correlations are consistently positive for all three metrics across model sizes, making them reasonable coarse, loss-aligned proxies for sample difficulty in our setting.

| Model Size | Word Frequency | Age of Acquisition | Verb Variation |
|----------------|----------------|--------------------|----------------|
| 14M | 0.717 | 0.611 | 0.780 |
| 31M | 0.723 | 0.611 | 0.773 |
| 70M | 0.734 | 0.618 | 0.768 |
| 160M | 0.734 | 0.615 | 0.755 |
| 410M | 0.745 | 0.627 | 0.746 |
| Average | 0.730 | 0.616 | 0.764 |

Table 5. Pearson Correlation of Linguistic Indices with Sample Loss.

Table 6. Word Frequency (Zipf) quantile excerpts. The extreme high-frequency tail can include repetitive or templated strings.

| Quantile | Typical form | Excerpt |
|----------|----------------------------|--|
| 25% | Dialogue / transcript-like | "Opening." "Welcome to the Montecito." [Crowd Chattering, Cheering] "All right, everybody, here we go." |
| 75% | Forum-style question | Is it OK to purchase cat food? Forgive a (possibly) silly question - but I have a cat as a pet, and of course I purchase cat food for him and feed it to him. |
| 100% | Keyword-stuffed tail | life insurance massachusetts long term care insurance illinois term life insurance quote insurance life life term whole health insurance ... |

Table 7. Word Age of Acquisition (AoA) quantile excerpts. The extreme AoA tail can include formulaic keyword lists.

E.4. Dataset Excerpts Across Curriculum Quantiles

We provide excerpts from the quantile inspection set used in §4.1. For word frequency, the low-frequency prefix often includes non-standard content such as source code, structured data, URLs, and non-English text, alongside technical writing with dense domain-specific terminology; mid-to-high frequency quantiles include narrative and conversational text as well as academic prose; and the extreme high-frequency tail can become dominated by repetitive strings. Consistent with Table 5, lower-frequency quantiles tend to have lower sample loss, while higher-frequency quantiles tend to have higher loss. AoA produces a related ordering: low-AoA regions include conversational or instructional English and non-linguistic content (e.g., code, numeric tables) when lexical coverage is limited; mid-range AoA samples include formal prose and documentation; higher-AoA samples often feature specialized academic or technical vocabulary. VV orders samples by detected verb-type diversity: low-VV quantiles include samples with few detected verbs (markup, lists, code); mid-range VV samples include formal expository prose; and the highest-VV tail frequently includes verb lexicons that inflate type counts.

E.5. The Zipf Scale for Word Frequency

The Zipf scale (Van Heuven et al., 2014) is a standardized, logarithmic measure of word frequency designed to be more intuitive than raw frequency counts or frequency per million words (fpmw). It is calculated as the base-10 logarithm of the frequency per billion words, which is equivalent to $\log_{10}(\text{fpmw}) + 3$. This transformation yields a scale (typically 1–7) that avoids the negative values and interpretation difficulties associated with fpmw for low-frequency words. The unit of the scale is the “Zipf”, and it provides a more linear representation of the word frequency effect in psycholinguistic studies.

F. Details of Probed Metrics

The evaluation suite includes science question answering, long-range context comprehension, logical reasoning, and commonsense understanding. Specifically, the AI2 Reasoning Challenge (ARC) (Clark et al., 2018) assesses science

| Quantile | Typical form | Excerpt |
|----------|----------------------------------|--|
| 0% | Markup / lists | <pre><li class="nav-group-task"> MBVisaRecognizerResult </pre> |
| 50% | Expository prose | To recognise always that the test of police efficiency is the absence of crime and disorder, and not the visible evidence of police action in dealing with them. |
| 100% | Verb lexicon / translation pairs | bautizar _to baptize, name_ beber _to drink_ bendecir _to bless_ beneficiar _to benefit, sell at a discount_ |

Table 8. Verb Variation (VV) quantile excerpts. VV should be interpreted as detected verb-type diversity; verb-list formats can dominate the extreme high-VV tail. URLs may be lightly redacted for readability.

| Name | Description |
|----------------------------------|---|
| Weight Dispersion Metrics | |
| L_1 | Average L_1 -norm over all weight matrices. |
| L_2 | Average L_2 -norm over all weight matrices. |
| L_1/L_2 | Average ratio of L_1 to L_2 norm (sparsity). |
| $\mu(w)$ | Sample mean of all weights. |
| median(w) | Median of all weights. |
| $\sigma(w)$ | Sample variance of all weights. |
| $\mu(b)$ | Sample mean of all biases. |
| median(b) | Median of all biases. |
| $\sigma(b)$ | Sample variance of all biases. |
| Layer Function Metrics | |
| trace | Average trace over all weight matrices. |
| λ_{max} | Average spectral norm over all weight matrices. |
| trace/ λ_{max} | Average ratio of trace to spectral norm. |
| $\mu(\lambda)$ | Average singular value over all matrices. |
| $\sigma(\lambda)$ | Sample variance of singular values over all matrices. |

Table 9. List of 14 metrics computed from model weights at each checkpoint, used as input for the HMM analysis.

question answering using both the Easy and Challenge subsets with accuracy measured via log-likelihood scoring. LAMBADA (Paperno et al., 2016) targets long-range context comprehension by requiring prediction of the final word in narrative passages. LogiQA (Liu et al., 2020) evaluates logical reasoning in reading comprehension with multiple-choice questions adapted from LSAT exams. PiQA (Bisk et al., 2020) measures commonsense physical reasoning via multiple-choice format. SciQ (Welbl et al., 2017) focuses on scientific question answering from educational materials. The Winograd Schema Challenge (WSC) (Levesque et al., 2012) tests commonsense pronoun resolution in minimally differing sentence pairs, and WinoGrande (Sakaguchi et al., 2021) extends this setting with an emphasis on robustness to dataset biases. Accuracy is used as the primary metric across these benchmarks.

G. HMM Weight Metrics

Following the methodology of Hu et al. (2023), we compute a set of 14 metrics from the network’s weights at each checkpoint to serve as the observation sequence for the HMM. These metrics are designed to capture properties of the weight distribution and the function computed by each layer. The full list is provided in Table 9.